Geoderma 462 (2025) 117549

Contents lists available at ScienceDirect

Geoderma

journal homepage: www.elsevier.com/locate/geoderma

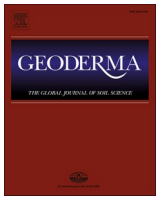

Effect of degree of saturation on the electrical conductivity of soils: role of surface conduction

Hyojung Ko [a], Heerym Han [b], Hyunwook Choo [b,*]

[a] Department of Civil and Environmental Engineering, 205 N Mathews Ave, University of Illinois, Urbana 61820, United States[1]
[b] Department of Civil and Environmental Engineering, Hanyang University, Seoul 04763, South Korea

ARTICLE INFO

Keywords:
Electrical conductivity
Degree of saturation
Archie's equation
Saturation exponent
Surface conduction

ABSTRACT

The estimation of the degree of saturation (S) based on electrical conductivity, σ_{mix} (or electrical resistivity) surveys typically relies on the S-exponent of Archie's equation. However, the S-exponent varies with soil type, indicating significant variability and the potential for miscalculation of S. This study focuses on the variability of the S-exponent in Archie's equation across soil types and investigates the relationship between σ_{mix} and S in terms of pore water conduction (K_w) and surface conduction (K_s) through theoretical modeling and experimentation. Silica sand and two types of clays were tested at various initial porosities and pore water concentrations, and σ_{mix} was measured over a range of S values (20% to 100%). For sand, where surface conduction is negligible, Archie's equation with a constant S-exponent (approximately 2) accurately predicted σ_{mix}. However, clays exhibited varying S-exponents, ranging from 1.5 to 2.1, depending on pore water conductivity. This suggests that a new model is needed to accurately predict σ_{mix} in unsaturated clayey soils. A newly proposed σ_{mix} estimation formula, incorporating separate S-exponents for K_w and K_s, provided accurate predictions across various test conditions. These findings enhance the understanding of electrical conductivity in unsaturated soils and offer a simple yet effective model for its prediction.

1. Introduction

The subsurface environment is a complex system of soil, water, and air, where the degree of water saturation (S), defined as the ratio of the volume of water to that of pore space, is a fundamental state variable governing a range of critical soil properties. The shift from saturated to unsaturated conditions significantly alters soil behavior, impacting its compressibility, strength, and hydraulic conductivity, as well as critical ecological and biogeochemical processes such as nutrient cycling, gas exchange, and microbial activity (Fredlund 2014; Gens 2010; Kohgo et al. 1993; McCarter et al. 2020; Mufti and Das 2023; Sheng 2011). Accurately quantifying S is therefore essential for understanding soil processes, including soil stability, water movement, solute transport, and a variety of biological and chemical activities within the soil profile.

While S can be directly measured (e.g., via gravimetric methods), these techniques are often destructive, time-consuming, and unsuitable for continuous monitoring. For this reason, various indirect techniques can be used to quantitatively assess S, including electrical resistivity (Mualem and Friedman 1991; Wahba et al. 2024; Zhou et al. 2015), gamma ray densitometry (Sharma et al. 2017), time domain reflectometry (Ozgur 2023), and neutron moderation (Falleiros et al. 1993). Among these, the electrical resistivity (or electrical conductivity) measurement technique has been widely adopted because electrical conduction in soils is primarily due to the migration of dissolved ions within the pore fluid and the diffuse double layer. This is because the majority of natural soil and rock matrices are electrically nonconductive, and a soil's electrical properties are therefore most sensitive to its fluid content and composition. This reflects that S is considered as the key feature determining the electrical conductivity of soils (Liu et al. 2022; Zhang et al. 2024). In addition, electrical conductivity measurements are continuous, sensitive, non-destructive, and reliable, and they show strong correlations with a range of other soil properties, such as porosity, salinity, soil texture, and temperature (Abu-Hassanein et al. 1996; Archie 1942; Brovelli et al. 2005; Choi et al. 2025; Franco-Luján et al. 2023; Kuranchie et al. 2014; Lee et al. 2021; Nocco et al. 2019; Sangprasat et al. 2024; Yang et al. 2024; Zhong et al. 2022; Zhou et al. 2015). The classic empirical model proposed by Archie (Archie 1942), which can be expressed as a power-function relationship between electrical

* Corresponding author.
E-mail address: choohw@hanyang.ac.kr (H. Choo).
[1] Formerly, graduate research assistant at Hanyang University.

https://doi.org/10.1016/j.geoderma.2025.117549
Received 12 May 2025; Received in revised form 30 September 2025; Accepted 8 October 2025
Available online 12 October 2025

conductivity and S with an exponent of approximately 2, has long been considered representative (Samouëlian et al. 2005). The original Archie's equation is given by:

$$\sigma_{mix} = \sigma_w n^m S^d \tag{1}$$

where σ_{mix} is the measured electrical conductivity of soils (or bulk electrical conductivity) in S/m, σ_w is the pore water conductivity in S/m, n is the porosity, m is the cementation exponent (or shape factor), and d is the saturation exponent. However, subsequent research has revealed that exponent d (denoted as saturation factor in Archie's equation) ranges from 1.4 to 2.3 depending on soil type (Abu-Hassanein et al. 1996; Chen et al. 2002; Keller and Frischknecht 1966; Schön 2015). This significant variability creates a fundamental challenge for accurate soil characterization. It suggests that a single, constant exponent may be an oversimplification, leading to inaccurate estimations of soil properties based on original Archie's equation.

The measured electrical conductivity in soils comprises two primary conduction pathways: pore water conduction (K_w), which is the electrical flow through the bulk pore water, and surface conduction (K_s), which is the electrical flow through the ion-enriched water of the diffuse double layer surrounding soil particles (Hasan et al. 2021). The relative contribution of these two pathways, and thus the overall electrical conductivity, is governed by the degree of water saturation (S). As S increases, pathways for electrical current are established and expanded in both the bulk pore water and the diffuse double layer, leading to an increase in both K_w and K_s (Liu et al. 2023). However, the mechanisms governing K_w and K_s in terms of S differ fundamentally due to the variation in conduction paths. Rashid et al. (2018) demonstrated that the conduction network for K_s through diffuse double layers is established at lower saturation levels than the network for K_w through interconnected pore water. This confirms that K_w and K_s in soils can exhibit different dependencies on S. Therefore, it was posited that the overall dependency of the measured σ_{mix} on S varies according to the relative magnitude between K_w and K_s.

This study aims to address the challenge of variable saturation exponent of Archie's equation by separating the two distinct conduction mechanisms in unsaturated soils. A central, testable objective is set to validate the hypothesis that the apparent variability of the saturation exponent is an artifact of a simplified model. It is hypothesized that by separating K_w and K_s using a theoretical framework, a constant, intrinsic exponent can be determined for each pathway, which will lead to a more accurate and robust model for soil electrical conductivity across a wide range of salinities and soil types. To achieve this, silica sand (K_w-dominant material) and two types of clays (kaolin and bentonite clays), which exhibit a significant contribution from K_s in a low-salinity pore water environment, were chosen as the testing materials. The σ_{mix} of three different types of soils with varying initial porosities and pore water concentrations was measured as a function of S, ranging from 20 % to 100 %. The measured σ_{mix} was separated into K_w and K_s based on a theoretical model, and the dependencies of K_w and K_s on S were investigated.

2. Theoretical framework

Electrical transport in a porous material can be represented by three resistances in parallel: particle resistance R_p, pore water resistance R_w, and surface resistance R_{sf} (Choo and Burns 2014). This model assumes that the soil particles are aligned in the direction of applied electrical field, as described by Klein and Santamarina (2003) and Pfannkuch (1972). Since the conductance is the inverse of resistance, the bulk electrical conductance (G_{mix}) can be expressed as

$$G_{mix} = G_p + G_w + G_{sf} \tag{2}$$

where G_p is particle conductance ($= 1/R_p$), G_w is pore water conductance ($= 1/R_w$), and G_{sf} is surface conductance ($1/R_{sf}$). Because most soil particles are insulators, the G_p of most geomaterials is negligible. Additionally, because conductance is a function of conductivity and the geometry of electrical current flow (Fig. 1), Eq. (2) becomes (Choo and Burns 2014):

$$\sigma_{mix}\frac{A}{L} = \sigma_w\frac{A_w}{L_e} + \sigma_s\frac{A_w}{L_e} \bullet G_s \bullet \rho_w \bullet S_a \bullet \frac{1-n}{n} \tag{3}$$

where σ_s is surface conductivity in S; A is total area; A_w is the area for pore water conduction; L is total length; L_e is the length of the water flow path; G_s is specific gravity; ρ_w is the mass density of water; S_a is the specific surface in m^2/g; and n is porosity. A_w in Eq. (3) can be expressed as (Fig. 1)

$$A_w = \frac{V_w}{V_T} \bullet \frac{A \bullet L}{L_e} = n \bullet S \bullet \frac{A \bullet L}{L_e} \tag{4}$$

where V_w is the volume for pore water conduction; V_T is total volume; and S is degree of saturation. Substitution of Eq. (4) into Eq. (3) yields:

$$\sigma_{mix} = K_w + K_s = \sigma_w\left(\frac{nS}{T^2}\right) + \sigma_s \bullet \left(\frac{(1-n)S}{T^2}\right) \bullet G_s \bullet \rho_w \bullet S_a \tag{5}$$

where K_w is pore water conduction (i.e., ionic conduction through continuous pore water), K_s is surface conduction (i.e., a special form of ionic conduction through the diffuse double layer), and T is tortuosity ($T = L_e/L$). When $S = 1$, Eq. (5) is identical to the formula derived by Choo and Burns (2014), and the detailed derivational process can be found in Choo and Burns (2014).

As the paths for K_w and K_s are not identical, separate tortuosity values can be employed for K_w and K_s (Choo et al., 2016a), and Eq. (5) can be rewritten as

$$\sigma_{mix} = K_w + K_s = \sigma_w\left(\frac{nS}{T_w^{\,2}}\right) + \sigma_s \bullet \left(\frac{(1-n)S}{T_s^{\,2}}\right) \bullet G_s \bullet \rho_w \bullet S_a \tag{6}$$

where T_w is the tortuosity for K_w, and T_s is the tortuosity for K_s. Previous studies attempted to correlate tortuosity with the porosity and degree of saturation of soils, as shown below (Chou et al. 2012; Millington and Quirk 1961). In these previous studies, T_w and T_s can be the power functions of n and S, respectively, as follows:

$$T_w = n^{-p}S^{-q} \tag{7-1}$$

$$T_s = n^{-p'}S^{-q'} \tag{7-2}$$

where *p, q, p', and q'* are fitting parameters. Substitution of (7) into Eq. (6) results in

$$\sigma_{mix} = \sigma_w n^{m_1} S^{d_1} + (1-n)n^{m_2} G_s \rho_w \sigma_s S_a S^{d_2} \tag{8}$$

where $m_1 = 1 + 2p$; $d_1 = 1 + 2q$; $m_2 = 2p'$; and $d_2 = 1 + 2q'$. Where the pore water has a high salinity (i.e., a very high σ_w) or the specific surface (S_a) of soils is very small (e.g., coarse-grained soils), the magnitude of K_w is much greater than that of K_s, leading to

$$\sigma_{mix} = \sigma_w n^{m_1} S^{d_1} \tag{9}$$

Because Eq. (9) is identical to the original Archie's equation (Eq. (1)), the empirically derived original Archie's equation has a strong theoretical background. The m_1 exponent in Eq. (9) indicates Archie's m exponent (Eq. (1)) or shape factor and typically ranges between 1.3 and 3.0 according to soil type and pore properties (i.e., shape and size of pore) (Archie 1942; Atkins and Smith, 1961; Salem and Chilingarian 1999). In addition, the d_1 exponent in Eq. (9) refers to the saturation factor (Eq. (1)).

The electrical conductivity of unsaturated soils with varying magnitudes of K_w and K_s can be captured by Eq. (8), but several complicated parameters (m_1, d_1, m_2, d_2, σ_s, and S_a) must be determined first. For practical applications, a simplified electrical conductivity formula with

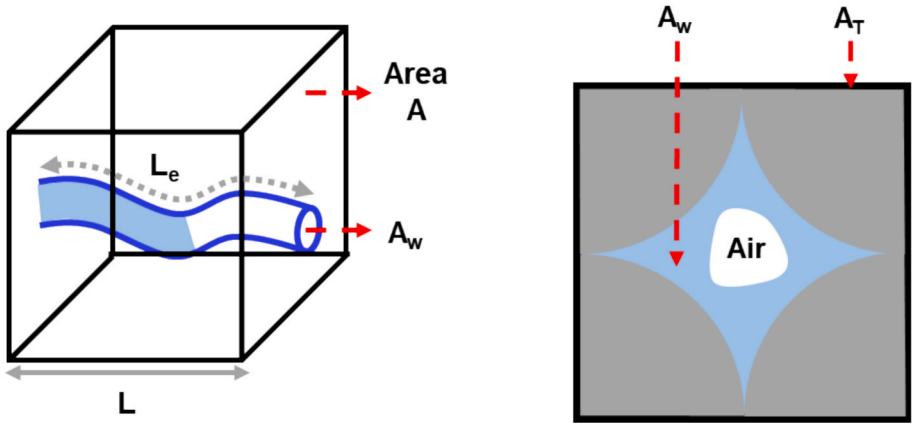

Fig. 1. Model for electronic transport phenomena in unsaturated soils.

a smaller number of input parameters may be preferable. Among the various formulas used to estimate electrical conductivity, the formula derived by Glover et al. (2000) is frequently used for saturated soils with significant surface conduction (Choo et al., 2016a):

$$\sigma_{mix} = K_w + K_s = \sigma_w n^m + \lambda(1 - n^m) \quad (10)$$

where λ is the matrix conductivity in S/m, capturing surface conductivity and the specific surface, and m is the shape factor, which is identical to the m exponent in Eq. (1) or m_1 exponent in Eq. (9). Choo et al. (2022) showed that the input parameters (m and λ) in Eq. (10) can be predicted by the soil index properties. However, as Eq. (10) is applicable only to saturated soils, to estimate σ_{mix} in unsaturated soils using Eq. (10), the effect of S must be considered. Because K_w in Eq. (10) obeys the original Archie's equation, which is consistent with Eq. (8), K_w in Eq. (10) for unsaturated soils can be expressed as $\sigma_w n^m S^{t_1}$, where t_1 is the saturation exponent for pore water conduction. In addition, based on the analogy between K_s in Eq. (8) and that in Eq. (10), K_s in Eq. (10) for unsaturated soils can be expressed as $\lambda(1 - n^m)S^{t_2}$, where t_2 is the saturation exponent for surface conduction. The extended Glover formula incorporating the effect of S then becomes

$$\sigma_{mix} = K_w + K_s = \sigma_w n^m S^{t_1} + \lambda(1 - n^m)S^{t_2} \quad (11)$$

When K_w is dominant over K_s, both Eq. (8) and Eq. (11) collapse to the original Archie's equation (Eq. (9)), and the m_1 and d_1 exponents in Eq. (8) are identical to the m and t_1 exponents in Eq. (11), respectively. However, due to the difference in the porosity function between Eq. (8) and Eq. (10), the d_2 and t_2 exponents may not be the same. Most importantly, Eq. (11), newly suggested in this study, includes separate saturation exponents for K_w and K_s (denoted as t_1 and t_2, respectively). Thus, the experimental results presented in this study are used to test the hypothesis that these saturation exponents are constant and intrinsic to the material, and that their separate contributions can be used to accurately predict the overall electrical conductivity of both coarse- and fine-grained soils across a wide range of water saturations and salinities.

3. Materials and methodology

3.1. Test materials

In this study, K-5 sand (from Kyung In Material Company, South Korea) was chosen as representative soil where pore water conduction is dominant (i.e., pore water conduction-dominant soil) due to the negligible surface conduction resulted from very small specific surface (Table 1) (Choo and Burns 2014). Meanwhile, kaolin clay (from Lakwoo Company, South Korea) and bentonite clay (from Donghae, South Korea) were selected as examples of soils where surface conduction prevails under conditions of low pore water salinity (i.e., surface conduction–dominant soils). According to the Unified Soil Classification System (USCS), K-5 sand was classified as poorly graded sand (SP), while kao.

lin and bentonite clays were categorized as low-plasticity clay (CL) and high-plasticity clays (CH), respectively. The index properties of the tested materials are listed in Table 1, and their chemical compositions are supplied in Table 2.

Table 1 also includes the index properties of AMK clay (manufactured by Active Minerals International), which was used for the electrical conductivity model verification. This material, a well-known type of kaolin clay, has been extensively studied by many previous researchers (Choo et al. 2022). Its surface properties, such as specific surface, are intermediate to those of the kaolin and bentonite clays tested in this study (Table 1), making it an ideal candidate for independent model verification. According to the USCS, AMK clay was categorized as CL.

3.2. Sample preparation and testing

The test matrix employed in this study is shown in Table 3. All tested materials were thoroughly washed at least six times with deionized (DI) water until the electrical conductivity of the supernatant was reduced to

Table 1
Index properties of tested materials.

Type	G_s	S_a (m^2/g)	e_{max}	e_{min}	LL (%)	PL (%)	Manufacturer
K-5 sand[1)]	2.65	0.03	1.07	0.69	–	–	Kyung In Material
Kaolin[2)]	2.53	10.92	–	–	36.4	23.6	Lakwoo Company
Bentonite[3)]	2.33	120.35	–	–	56.6	35.5	Donghae Chemicals
AMK clay[4)]	2.60	49.4	–	–	59.8	25.5	Active Minerals
Testing method	ASTM D854	[1)] Empirical equation; [2), 3), 4)] Methylene blue spot test (Santamarina et al. 2002)	ASTM D4254	ASTM D4253	BS 1377	ASTM D4318	

Note: G_s = specific gravity; S_a = specific surface; e_{max} = maximum void ratio; e_{min} = minimum void ratio; LL = liquid limit; PL = plastic limit.

Table 2
Chemical composition of tested clays.

Type	Al_2O_3	CaO	Fe_2O_3	K_2O	MnO	Na_2O	P_2O_5	SiO_2	TiO_2	LOI
	Weight (%)									
Kaolin	34.01	5.51	1.32	0.48	0.01	1.72	0.01	47.66	0.16	8.74
Bentonite	15.96	1.62	2.97	2.72	0.12	1.20	0.08	61.98	0.43	10.8

Note: Fe_2O_3 = total Fe; LOI = loss of ignition

Table 3
Sample preparation method and testing program.

Type		K-5 Sand	Kaolin clay	Bentonite clay
Saturated condition ($S = 1$)	Sample preparation	Water pluviation	Slurry mixing	
	Initial porosity	0.45($Dr = 60$ %), 0.49($Dr = 30$ %)	0.47 (1.5LL) – 0.82 (5.0LL)	0.66(1.5LL) – 0.87(5.0LL)
	σ'_v (kPa)	1.85 – 416.39 ($LIR = 1$)	–	–
	σ_w (S/m)	0.057, 1.88, 4.20	0.012 – 11.20	0.012 – 4.20
Unsaturated condition ($S = 0.2$ – 0.9)	Sample preparation	Compaction		
	Initial porosity	0.45($Dr = 60$ %), 0.49($Dr = 30$ %)	0.41 – 0.82	0.56 – 0.70
	σ'_v (kPa)	1.85 – 416.39 ($LIR = 1$)	–	–
	σ_w (S/m)	0.057, 1.88, 4.20	0.012 – 4.20	0.012 – 4.20

Note: S = degree of saturation; LL = liquid limit; Dr = relative density; σ_w = pore water conductivity; σ'_v = applied vertical effective stress; LIR = load increment ratio.

below 0.001 S/m. This process was employed to remove any unknown ions and salts attached to the surface of the soil particles (Choo et al., 2016b). The rinsed soils were then oven-dried and stored in a sealed container to control the initial water content according to the test matrix in Table 3. The water pluviation method with symmetric tapping was used to prepare the saturated sand specimens with initial relative densities of 30 % and 60 % (Table 3). Vertical stress of up to 416.4 kPa was then applied to vary the porosity, and the resulting electrical conductivity was measured as a function of the change in porosity. In the case of unsaturated sand specimens, the dry sand was mixed with water to achieve gravimetric water contents ranging from 7 % to 28 %. The wet soil was then compacted under varying compaction energies to prepare specimens with initial relative densities of 30 % and 60 % and degrees of saturation ranging from 20 % to 80 %. Vertical stress up to 416.4 kPa was then applied. The electrical conductivity was measured under three different pore water conductivities (σ_w) of 0.057, 1.88, 4.20 S/m (Table 3).

The slurry mixing method was employed to prepare the saturated clay specimens. The initial water content of the specimen was determined as being between 1.5 and 5.0 times the liquid limit of the clays being tested (Table 3). To prepare unsaturated clay specimens with varying dry unit weights and degrees of saturation (S), standard compaction tests were performed first (Fig. 2). Based on the lines of saturation in Fig. 2, specimens were prepared with S values ranging from 45 % to 80 % and dry unit weights ranging from 7.8 kN/m^3 to 13.4 kN/m^3. Different compaction energies were applied to the unsaturated soils by varying the number of hammer blows in order to achieve the target dry unit weights at a given water content. The number of hammer blows was determined through trial and error. The electrical conductivity was measured under varying σ_w ranging from 0.012 to 11.2 S/m (0.001 to 1.5 M NaCl). Both unsaturated sand and saturated and unsaturated clays

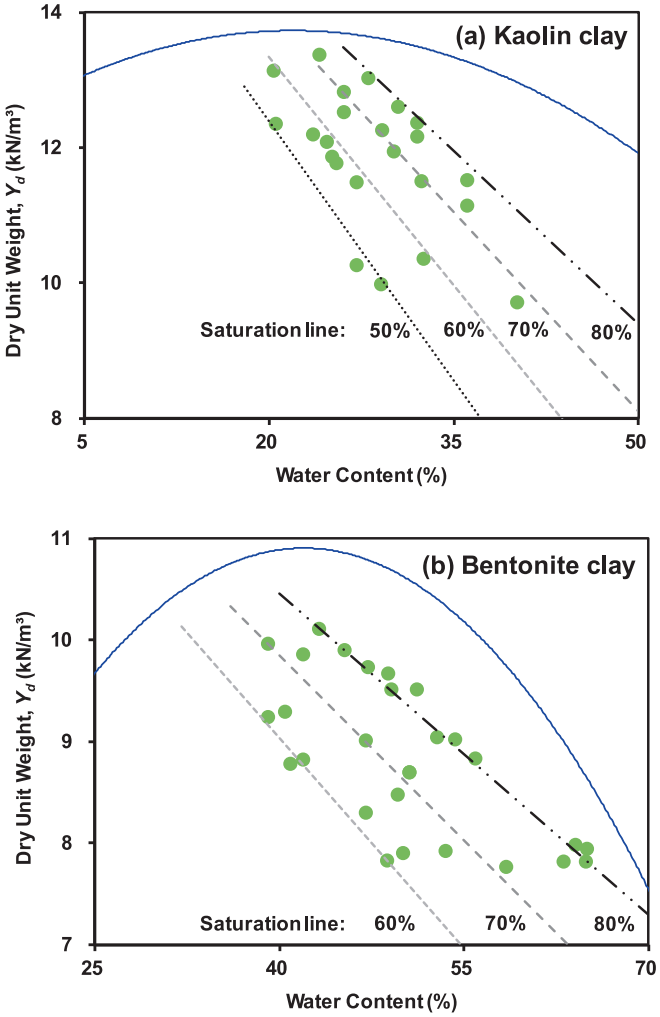

Fig. 2. Compaction curve and line for degree of saturation for tested unsaturated clayey soils. Note the filled symbols indicate test conditions for the unsaturated clays.

were stored in plastic bags for one day before electrical conductivity measurements to ensure even distribution of water.

3.3. Test equipment and measurement

To assess the electrical conductivity of the specimens, we utilized a modified oedometer cell that incorporated a novel four-electrode conductivity probe, as depicted in Fig. 3. The inside of the cell was constructed from non-conductive polyvinyl chloride for electrical insulation. The specimen had a diameter of 100 mm and a height of 70 mm. The four-electrode conductivity probe, which consisted of high-current (Hc), low-current (Lc), high-potential (Hp), and low-potential (Lp) electrodes, was designed to overcome the limitations of conventional four-electrode arrays that tend to provide only localized measurements. In our unique configuration, the Hc and Hp electrodes were

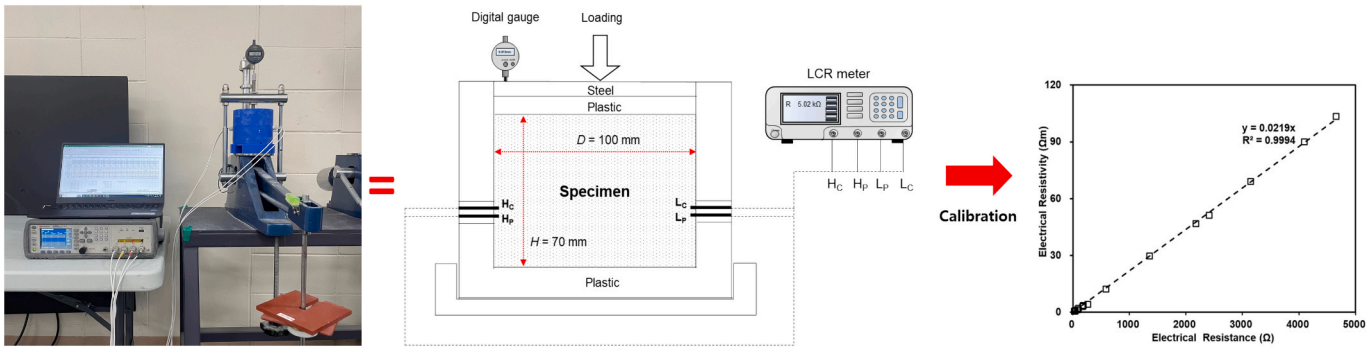

Fig. 3. Test setup for electrical conductivity/resistivity measurement. For the calibration of the 4-electrode system, the electrical resistivity was measured using a conductivity meter (Accumet Excel XL200) and electrical resistance was measured using an LCR meter (Keysight E4980). H_c = high current; H_p = high potential; L_p = low potential; and L_c = low current.

placed in close proximity on one side of the specimen, while the Lc and Lp electrodes were similarly grouped on the opposite side. This arrangement forces the electrical current to flow through the entire bulk of the specimen, thereby allowing for the measurement of the global electrical conductivity of the tested soil.

During the experiments, the potential differences between Hp and Lp were measured to determine electrical resistance using an LCR (inductance, capacitance, and resistance) meter. The input voltage of the LCR meter was set to 1 V, and an operating frequency of 10 kHz was chosen to avoid electrical resonance and electrode polarization. The measured electrical resistance was then converted to electrical conductivity (the reciprocal of electrical resistivity) using the calibration factor obtained from experiments on NaCl solutions of varying concentrations (Fig. 3). The measured electrical conductivity of each specimen was used to validate our theoretical model (Eq. (11)) and to test our central hypothesis that the separate *S*-exponents (i.e., t_1 and t_2) are constant and intrinsic to the material rather than being variable.

4. Results and analysis

The primary objective of this section is to present and analyze the experimental results to validate our theoretical framework. Our central hypothesis, that the apparent variability of the saturation exponent in existing models is an artifact of a simplified framework that fails to separate the effects of pore water and surface conduction, will be tested here. To determine the t_1 and t_2 exponents, the determination of the m exponent is a prerequisite (Eq. (11)). Therefore, the following section starts by showing the electrical conductivity of sand, a pore water conduction-dominant material, in both saturated and unsaturated conditions, followed by the electrical conductivity of clays in both saturated and unsaturated conditions.

4.1. Electrical conductivity of sand

4.1.1. Saturated condition

The measured electrical conductivity (σ_{mix}) of the tested saturated sand increased with both porosity (n) and pore water conductivity (σ_w) (Fig. 4(a)). This indicates an increase in pore water conduction, as shown in Eq. (10) (Ko et al. 2023). Fig. 4(b) depicts the normalized electrical conductivity (σ_{mix}/σ_w) of tested sand according to n. To analyze the measured σ_{mix} in Fig. 4(a), the normalized conductivity was defined as follows based on Eq. (11):

$$\sigma_{mix}/\sigma_w = n^m S^{t1} + \lambda/\sigma_w \bullet (1 - n^m) S^{t2} \quad (12)$$

For saturated soils (i.e., degree of saturation, $S = 1$), Eq. (12) becomes

$$\sigma_{mix}/\sigma_w = n^m + \lambda/\sigma_w \bullet (1 - n^m) \quad (13)$$

Regardless of the concentration of pore water, σ_{mix}/σ_w can be expressed

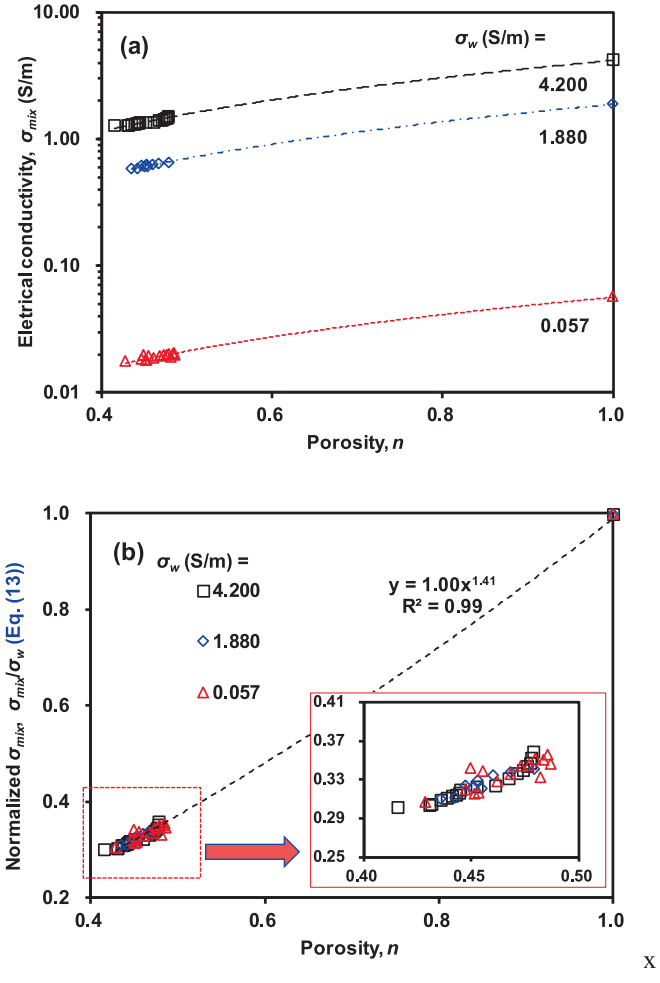

Fig. 4. Variations in (a) bulk electrical conductivity (σ_{mix}) and (b) normalized electrical conductivity of the saturated sand as a function of porosity (n) under three different pore water conductivities. The dashed line in figure (b) indicates the non-linear line of best fit for the measured data. Therefore, the normalized σ_{mix} (Eq. (13) can be simplified as n^m, confirming the pore water conduction dominance.

as a single function of n, as shown in Fig. 4(b), indicating that λ/σ_w in Eq. (13) can be assumed to be zero for the tested sand and the m exponent is not affected by the concentration of pore water. Thus, the electrical conductivity of the tested sand in a saturated condition can be described by Eq. (1) or Eq. (9) (Archie's equation). This implies that the dominant mechanism for electrical conduction in this sand is through the pore

water, while surface conduction plays a negligible role.

4.1.2. Unsaturated condition

Fig. 5 shows the measured σ_{mix} of the tested sand with varying S as a function of n in both high-salinity (Fig. 5(a)) and low-salinity (Fig. 5(b)) water environments. Similar to the results for the saturated condition (Fig. 4), Fig. 5(a) and Fig. 5(b) demonstrate that the σ_{mix} of tested unsaturated sand increased with n because of the significance of pore water conduction. In addition, at a given n, σ_{mix} increased with S because S determines the connectivity of a continuous electrical flow network and controls the electrical pathways through a porous system (Kułynycz 2017; Liu et al. 2023; Scarfone et al. 2020; Yang et al. 2024). To evaluate the dependency of σ_{mix} of tested unsaturated sand on porosity (n), the normalized conductivity, expressed by Eq. (12), is plotted as a function of n in Fig. 5(c). This reveals that σ_{mix}/σ_w can be expressed as a single function of n at a given S regardless of pore water conductivities, implying that the σ_{mix} of tested unsaturated sand is determined by pore water conduction (Eq. (12)). Additionally, at a given n, the normalized conductivity decreased with S; however, the m exponent (for porosity) remained at an almost constant value of 1.41, which is identical to the m exponent of saturated sand in Fig. 4(b). This observation confirms that the porosity exponent m in Eq. (11) or Eq. (12) is not affected by S. Although the constancy of the exponent m was not the central hypothesis being tested in this study, this finding demonstrates that the effects of porosity and saturation can be effectively decoupled in the developed electrical conductivity model (Eq. (11)).

To examine the impact of S on the σ_{mix} of tested sand, the ratio of σ_{mix} in an unsaturated condition to that in a saturated condition (unsat-sat conductivity ratio) was defined in this study as

$$\frac{\sigma_{mix}(unsaturated)}{\sigma_{mix}(saturated)} = \frac{\sigma_w n^m S^{t1} + \lambda(1-n^m)S^{t2}}{\sigma_w n^m + \lambda(1-n^m)} \quad (14)$$

The tested sand is a pore water conduction–dominant material (i.e., $K_w \gg K_s$); thus, Eq. (14) can be simplified as follows to define unsat-sat K_w ratio

$$\frac{\sigma_{mix}(unsaturated)}{\sigma_{mix}(saturated)} = \frac{\sigma_{mix}(unsaturated)}{\sigma_w n^m} = S^{t1} \qquad \text{when } K_w >> K_s \quad (15)$$

Fig. 6 shows the variation of unsat-sat conductivity (or K_w) ratio (Eq. (15)) according to S. Based on Fig. 4, the m exponent in Eq. (15) was 1.41, and Fig. 6 shows that the unsat-sat conductivity ratio is a sole power function of S, with a t_1 exponent of approximately 1.91. This reflects the relevance of Eq. (15) and reconfirms that the tested sand is a pore water conduction–dominant material with negligible surface conduction. The determined t_1 exponent in Eq. (15) was comparable to that of previous studies (Hamada 2010; Mualem and Friedman 1991; Pirson 1963). Consequently, the electrical conductivity of pore water conduction–dominant materials such as coarse grains and marine sediments can be accurately captured by the original Archie's equation, using Eq. (1) or Eq. (9), with constant porosity and saturation exponents regardless of pore water conductivity.

4.2. Electrical conductivity of saturated clay

Fig. 7(a) and (b) show the variations in the measured σ_{mix} of tested saturated clayey soils at varying σ_w as a function of n. Different from the results of sand in Fig. 4, the relationships between σ_{mix} and n varied with σ_w: 1) when σ_w was high (i.e., $\sigma_w \geq 0.049$ S/m), σ_{mix} increased with increasing in n; and 2) when σ_w was low (i.e., $\sigma_w < 0.049$ S/m), σ_{mix} decreased with increasing n. These opposite variations of σ_{mix} according to n can be attributed to the increase in pore water conduction (K_w) and decrease in surface conduction (K_s) with increasing n as indicated by Eq. (10) (Ko et al. 2023). Note, for the kaolin clay, a wider range of nine pore water conductivities was tested to fully characterize the nonlinear relationship between the apparent cementation exponent and pore fluid

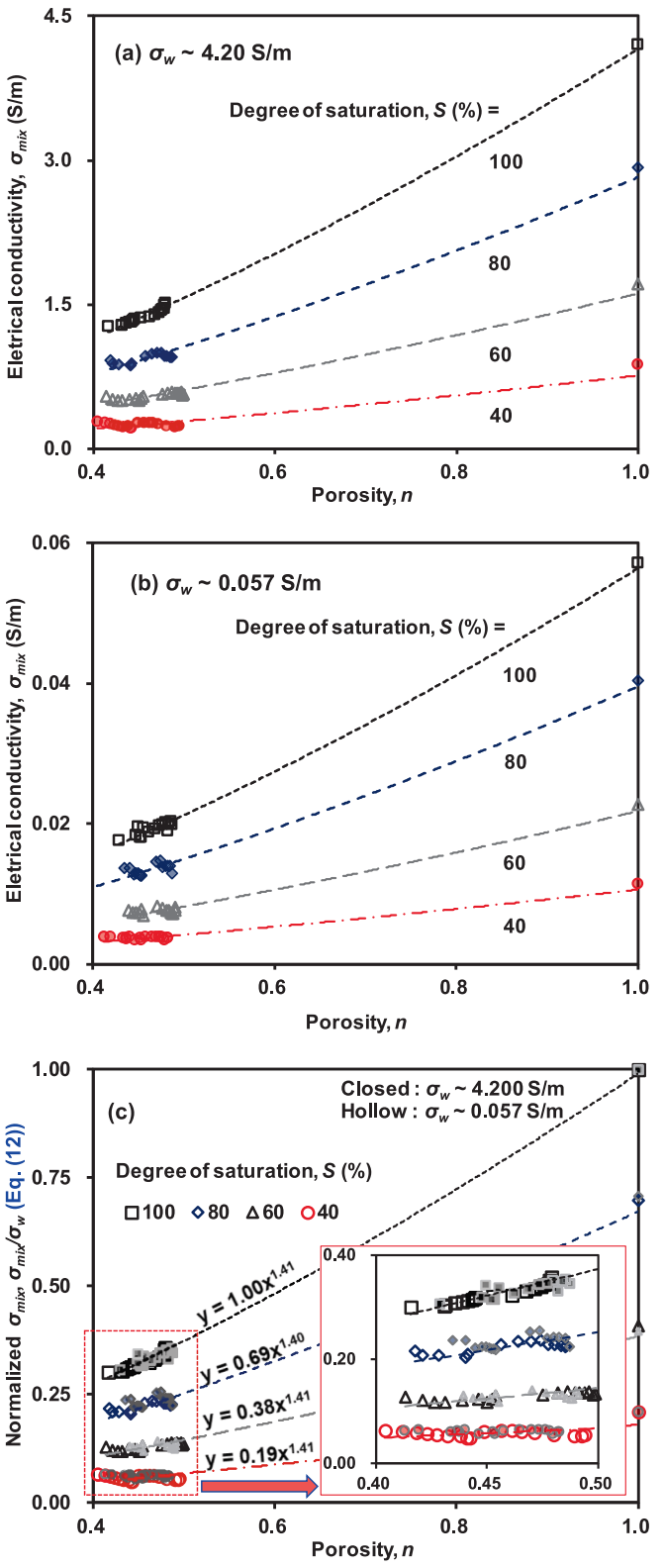

Fig. 5. Variations in (a and b) bulk electrical conductivity (σ_{mix}) and (c) normalized electrical conductivity of the unsaturated sands with varying degrees of saturation as a function of porosity (n) at different pore water conductivities: (a) σ_w ~ 4.200 S/m and (b) σ_w ~ 0.057 S/m. Note that the degree of saturation (S) indicated in the figures above represents the target values during sample preparation. The measured S of each test specimen slightly deviated from the target S. Therefore, for model development, the measured S was used. The dashed lines in figure (c) indicate the non-linear line of best fit for the measured data at each S value.

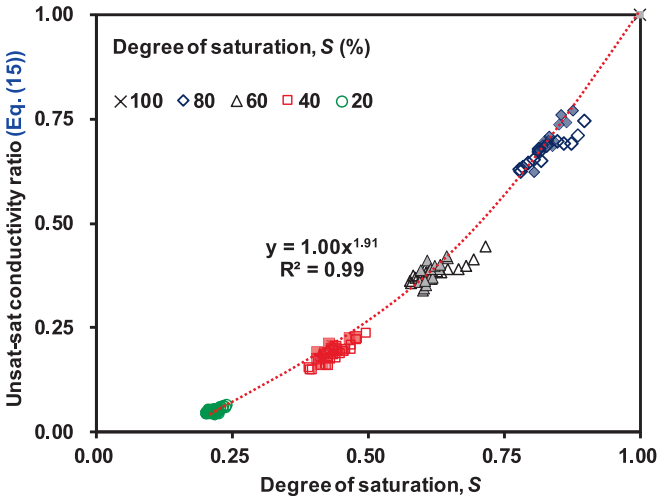

Fig. 6. The ratio of measured electrical conductivity of the tested sand in unsaturated condition to that in saturated condition ($\sigma_{mix(unsat)}/\sigma_{mix(sat)}$) as a function of degree of saturation (Equation (14) or (15)). The dashed line indicates the non-linear line of best fit for the measured data, and the obtained equation of the trendline supports the relevance of Equation (15).

salinity. In contrast, for the bentonite clay, a more limited range of two conductivities (0.012 and 4.2 S/m) was used, as the primary goal was to demonstrate the pronounced effects of surface conduction in a high specific surface clay at both low and high salinity extremes.

Fig. 7(c) and (d) show the variations in the normalized electrical conductivity (Eq. (13)) of tested saturated clays as a function of n. Fig. 7 (c) and Fig. 7(d) illustrate that: 1) when the pore water has low salinity, the normalized conductivity increased with decreasing σ_w at a given n due to the increase in λ/σ_w, reflecting the significance of K_s; and 2) when the pore water has high salinity, the normalized conductivity can be represented as a single function of n that is almost consistent regardless of σ_w due to the negligible λ/σ_w, indicating the predominance of K_w. Additionally, as can be seen in Fig. 7(c) and Fig. 7(d), due to the opposing dependencies of K_w and K_s according to n, the overall dependency of σ_{mix}/σ_w on n can be determined by the relative magnitudes of K_w and K_s. When K_s was greater than K_w ($\sigma_w < 0.049$ S/m), the normalized conductivity decreased with an increasing n, and when K_w was greater than K_s ($\sigma_w \geq 0.049$ S/m), the normalized conductivity increased with n.

Although Fig. 7 clearly reveals the importance of K_s for the tested clayey soils, particularly at low pore water conductivities, it was assumed that the measured σ_{mix} can be captured by Eq. (9) (original Archie's equation). Therefore, the power relation between normalized conductivity and porosity was established using the data in Fig. 7(c). The determined Archie's m (or m_1) exponent (i.e., the apparent cementation exponent) was plotted as a function of σ_w in Fig. 8, which shows that the m exponent in the tested kaolin clays increased rapidly with increasing σ_w at low σ_w. However, the rate of increase in the m exponent with σ_w decelerated, approaching an asymptotic m value of 2.15 ($\sigma_w > 2.680$ S/m). This almost constant m exponent at a high σ_w

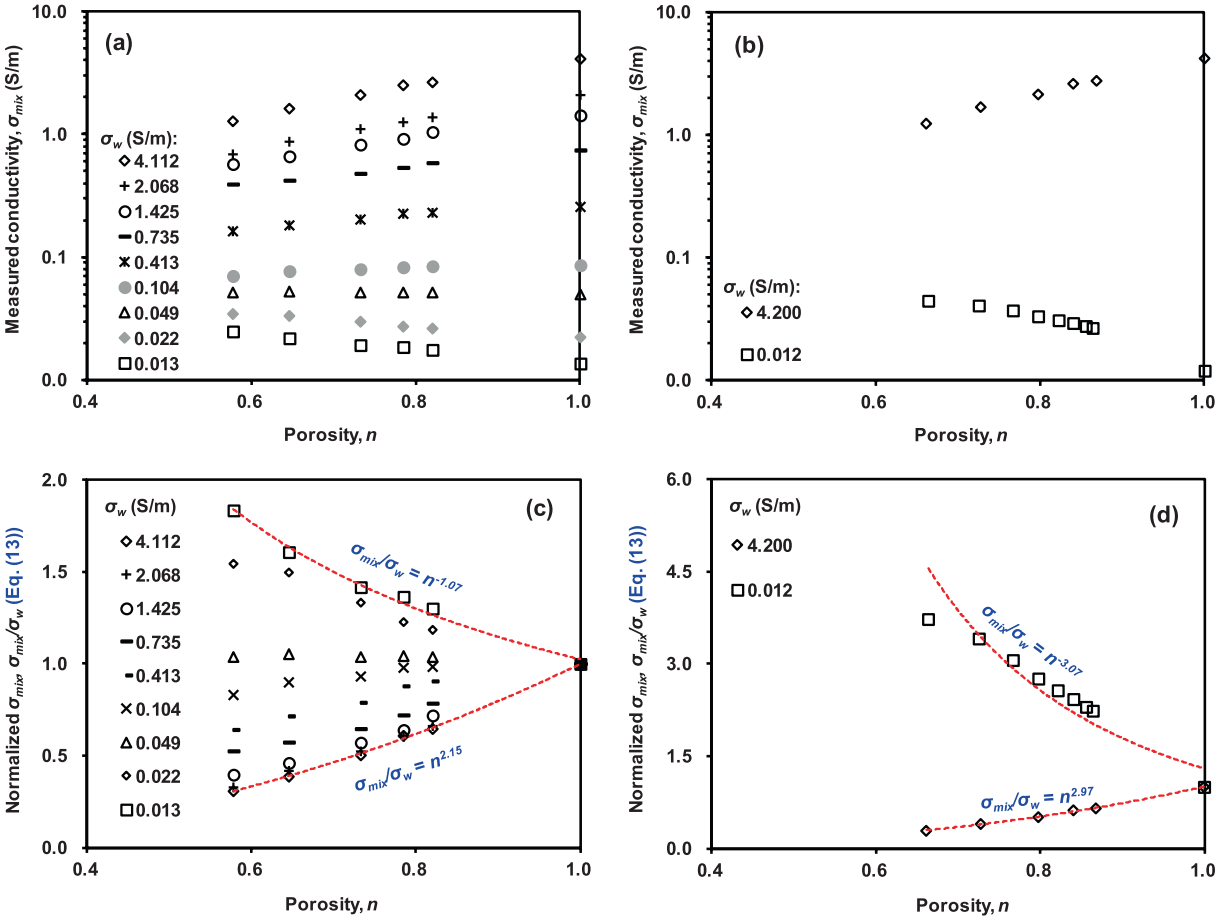

Fig. 7. Variations in (a and b) bulk electrical conductivity (σ_{mix}) and (c and d) normalized electrical conductivity of the tested saturated clays as a function of porosity (n) at varying pore water conductivities: (a and c) kaolin clay; (b and d) bentonite clay. Note the pore water conductivities (σ_w) were controlled by NaCl molar concentration: 0.5 M NaCl solution = 4.112 S/m; 0.3 M = 2.068 S/m; 0.2 M = 1.425 S/m; 0.1 M = 0.735 S/m; 0.01 M = 0.084 S/m; 0.005 M = 0.049 S/m; 0.002 M = 0.022 S/m; and 0.001 M = 0.012 S/m. The dashed lines in figures (c) and (d) indicate the modeled values based on the original Archie's equation (Eq. (9)).

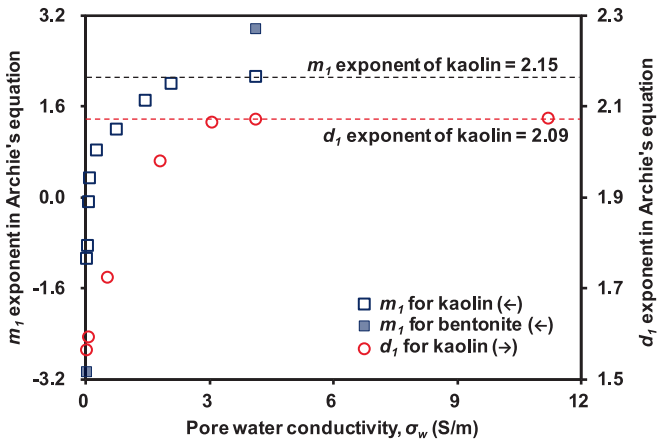

Fig. 8. Variations in m_1-exponent (i.e., apparent cementation exponent) and d_1-exponent (i.e., exponent for degree of saturation) in Archie's equation (Equation (9)) of tested kaolin clays as a function of pore water conductivity.

shows that the magnitude of K_w is significantly greater than that of K_s. In contrast, for the kaolin clay at a relatively low σ_w, the determined m exponent was not constant, indicating that the original Archie's equation cannot consider K_s (Choo et al., 2016a). Finally, the tested bentonite had a smaller m exponent at a low σ_w but a greater m exponent at a high σ_w compared with kaolin clay due to the greater specific surface (Choo et al. 2022).

4.3. Electrical conductivity of unsaturated clay

4.3.1. Electrical conductivity according to pore water conductivity

To examine the dependency of the measured σ_{mix} on degree of saturation (S), σ_{mix} of the tested kaolin clay with varying pore water conductivities (σ_w) was plotted as a function of S in Fig. 9(a). To isolate the impact of n on the measured σ_{mix}, all tested materials were prepared under a similar n (approximately 0.50). Fig. 9(a) clearly indicates that the σ_{mix} of the tested clay increased with S and σ_w. Although the measured σ_{mix} of clayey soils is determined by both pore water conduction (K_w) and surface conduction (K_s), as demonstrated in the previous section, it was assumed that Eq. (9) can capture the measured σ_{mix} of tested unsaturated kaolin clay. Under this assumption, the unsat-sat conductivity ratio can be expressed by Eq. (15), and the t_1 exponent in Eq. (15) can be replaced with the d_1 exponent in the original Archie's equation (Eq. (9)). The measured conductivity data in Fig. 9(a) were normalized with conductivity at $S = 1$ (i.e., the determination of unsat-sat conductivity ratio in Eq. (15)), and the determined unsat-sat conductivity ratio was plotted according to S in Fig. 9(b). Fig. 9(b) shows that tested kaolin clays with varying σ_w can be expressed as a power function of S; however, the d_1 exponent in Eq. (9) varied with σ_w.

Fig. 8 shows the variation of the determined d_1 exponent in Eq. (9) (i.e., the exponent for S in Archie's equation) as a function of σ_w. As shown in Fig. 8, the d_1 exponent increased nonlinearly from 1.56 to 2.09 with increasing σ_w, reflecting that the change in σ_w and the consequent change in the relative magnitudes between K_w and K_s influence the overall dependency of σ_{mix} on S. This hypothesis is further supported by the experimental results of Bai et al. (2013), who found that the dependency of σ_{mix} of compacted lateritic soil on S varied with the initial density of the tested soils. The range of the d_1 exponent determined in this study was comparable with that of previous studies that examined varying soil types (Abu-Hassanein et al. 1996; Chen et al. 2002; Keller and Frischknecht 1966; Schön 2015). Because soil type, including clay fraction, determines the relative magnitudes between K_w and K_s at a given pore water conductivity, the results of this study and previous studies indicate a difference in dependency of K_w and K_s on S. Thus, a new model is required to capture the electrical conductivity of

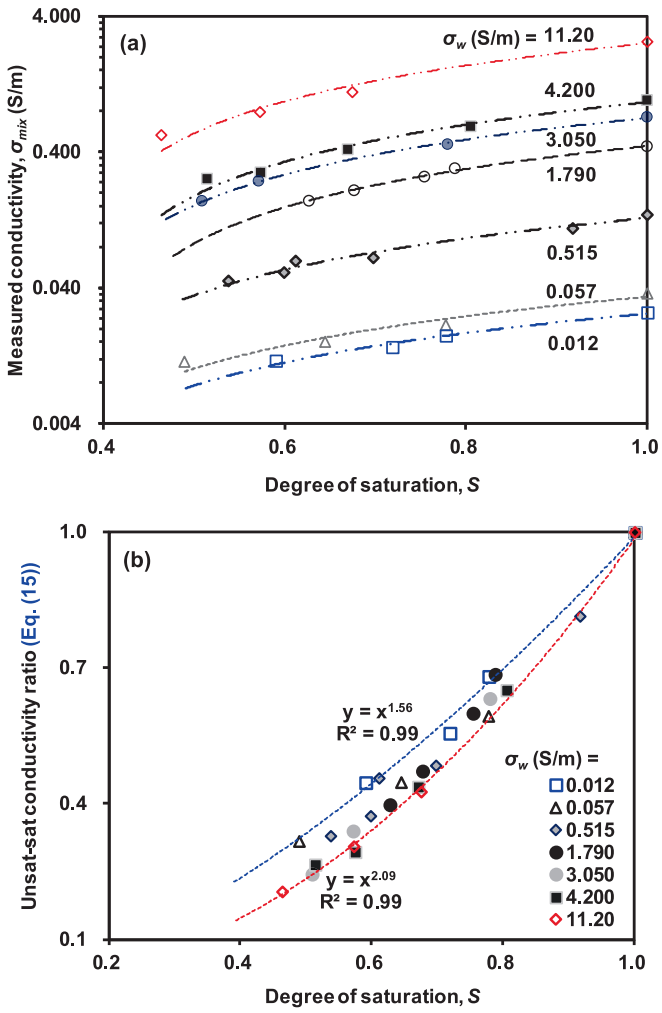

Fig. 9. Variations in (a) measured electrical conductivity (σ_{mix}) and (b) the ratio of measured electrical conductivity in unsaturated condition to that in saturated condition ($\sigma_{mix(unsat)}/\sigma_{mix(sat)}$) of the tested kaolin clays as a function of degree of saturation at varying pore water conductivities. Note that the porosity of all tested materials shown in the figure was similar, approximately 0.50. The dashed lines in figure (b) indicate the modeled values based on the original Archie's equation (Eq. (15)). The determined S exponents shown range from 1.56 (at $\sigma_w = 0.012$ S/m) to 2.09 (at $\sigma_w = 11.20$ S/m).

unsaturated soils, with greater emphasis on surface conduction.

At high σ_w (> 3.05 S/m), the d_1 exponent remained at an almost constant value of approximately 2.09. The constant d_1 exponent and m_1 exponent occurred at similar σ_w (Fig. 8), confirming that Eq. (9) can accurately predict the electrical conductivity of unsaturated soils with negligible surface conduction (Talabani et al. 2000).

4.3.2. Electrical conductivity of unsaturated clayey soils in high-salinity pore water

Fig. 10(a) and (b) depict the variation of the normalized σ_{mix} as expressed by Eq. (12) of the tested clays with varying values of S as a function of n in a high-salinity water environment ($\sigma_w \sim 4.2$ S/m). Because the λ/σ_w in Eq. (12) can be assumed to be zero for the tested clays at very high σ_w, the normalized σ_{mix} in Fig. 10(a) and Fig. 10(b) indicates $n^m S^{t_1}$. Thus, the normalized σ_{mix} in Fig. 10(a) and Fig. 10(b) increased with S at a given n, reflecting the formation of an electrical conduction path with increasing S, and the normalized σ_{mix} at a given S can be expressed as a power function of n, similar to Eq. (9). In particular, the determined m exponent (for porosity) is comparable with that of tested clay in saturated conditions (Fig. 8) regardless of S,

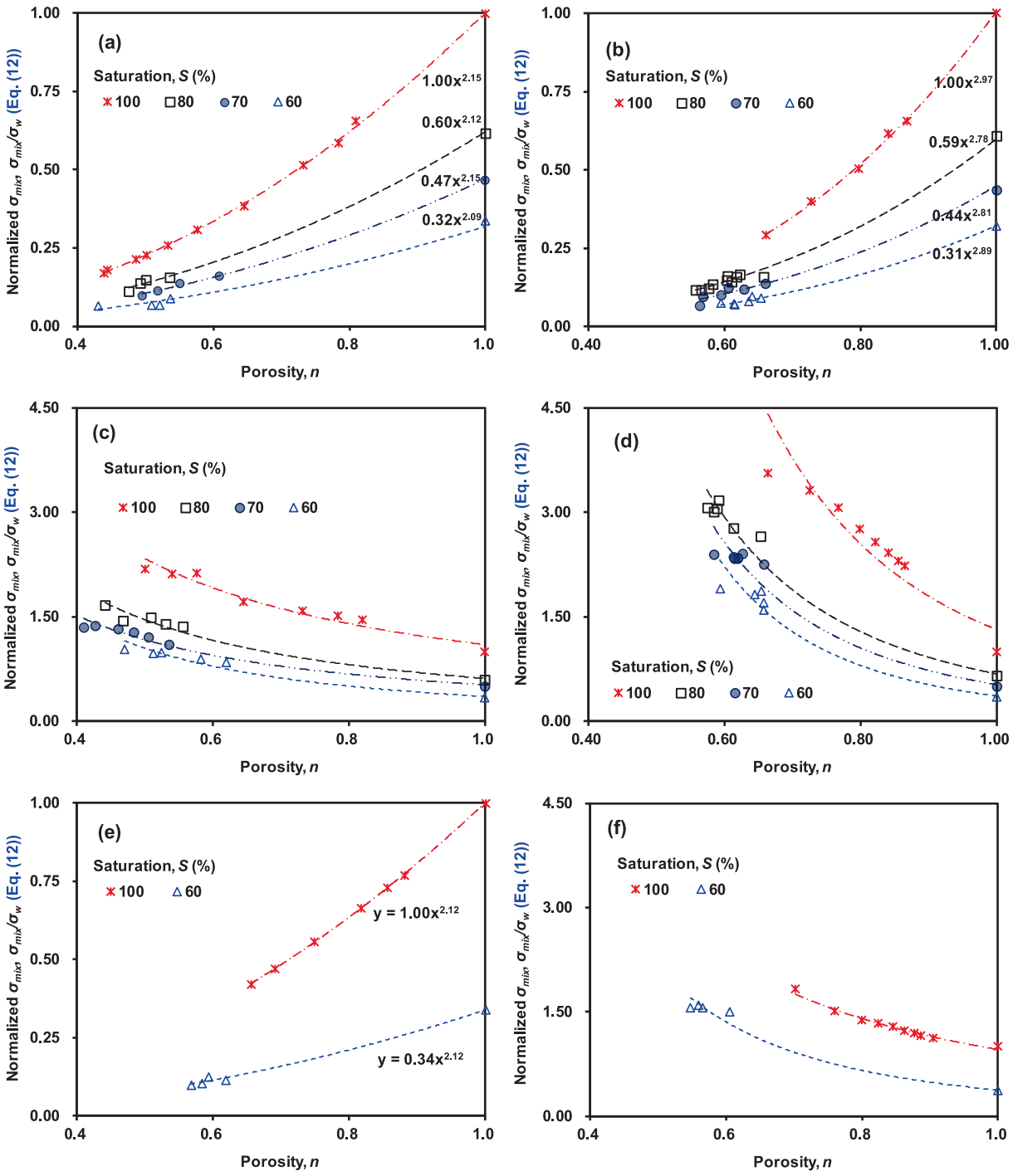

Fig. 10. Variations in the normalized electrical conductivity of the tested clayey soils with varying degrees of saturation as a function of porosity: (a) kaolin clay at pore water conductivity (σ_w) = 4.2 S/m; (b) bentonite clay at σ_w = 4.2 S/m; (c) kaolin clay at σ_w = 0.012 S/m; (d) bentonite clay at σ_w = 0.012 S/m; (e) AMK clay at σ_w = 4.2 S/m; and (f) AMK clay at σ_w = 0.012 S/m. The dashed line indicates the non-linear line of best fit for the measured data, and the obtained equations of the trendline in figures (a), (b), and (e) support the relevance of Archie's equation.

reconfirming that the exponent m in Eq. (11) or Eq. (12) is not affected by S.

Because the tested clays at a high σ_w are pore water conduction-dominant materials, the unsat-sat conductivity ratios (Eq. (15)) of tested kaolin and bentonite clays were plotted as a function of S in Fig. 11(a) to examine the impact of S on K_w. The unsat-sat conductivity ratio can be expressed as a power function of S, with exponents of approximately 2.09 for tested kaolin clay and 2.41 for tested bentonite clay. The findings depicted in Fig. 10 and Fig. 11 reveal that K_w (or σ_{mix} at a high σ_w) of tested clays obeys the original Archie's equation, as expressed by Eq. (9), with constant m and t_1 exponents, leading to

$$K_w = \sigma_w n^m S^{t_1} \tag{16}$$

The determined m and t_1 exponents for the tested clays are given in Table 4.

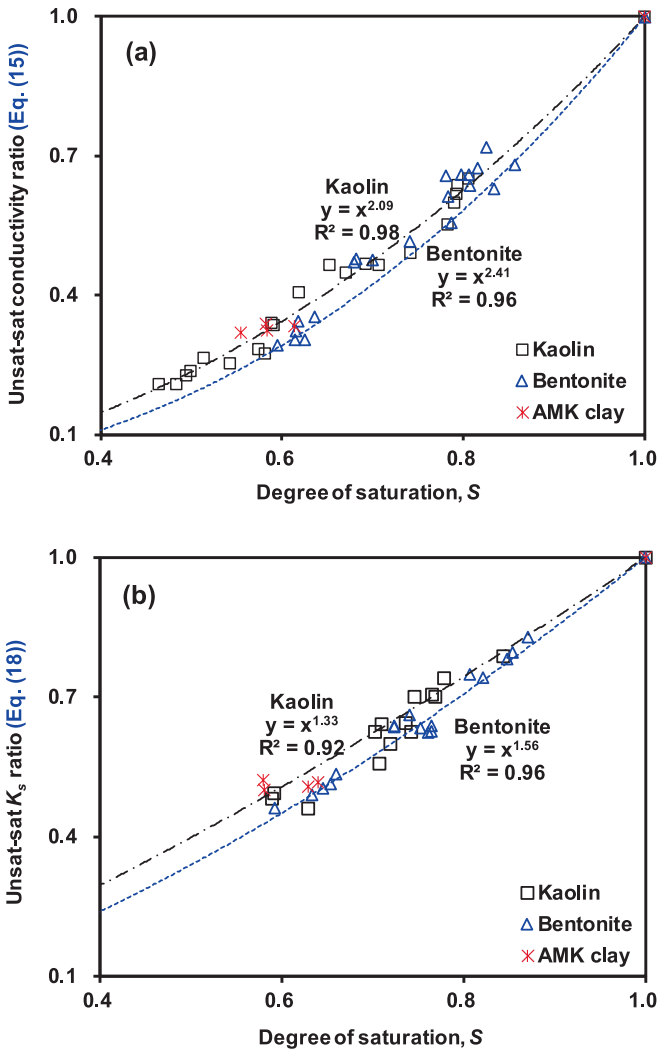

Fig. 11. Variations in (a) unsaturated–saturated electrical conductivity ratio ($\sigma_{mix(unsat)}/(\sigma_{mix(sat)}$) (Equation (15)) and (b) unsaturated–saturated surface conduction ratio ($K_{s(unsat)}/(K_{s(sat)}$) (Equation (18)) of tested clays as a function of degree of saturation. The dashed line in figure (a) indicates Eq. (15) and that in figure (b) indicates Eq. (18).

Table 4
Input parameters (*m*, t_1, *and* t_2 exponents) for Equation (11).

Type	*m*	t_1	t_2
Kaolin	2.15	2.09	1.33
Bentonite	2.97	2.41	1.56

4.3.3. *Electrical conductivity of unsaturated clayey soils in low-salinity pore water*

Fig. 10(c) and (d) depict the variation of the normalized electrical conductivity (σ_{mix}) (Eq. (12)) of the tested clays with varying *S* as a function of *n* in a low-salinity water environment ($\sigma_w \sim 0.012$ S/m). Similar to the behavior of the tested clays in saturated condition with low σ_w (Fig. 7), the normalized σ_{mix} decreased as *n* increased at a given *S*, indicating the significance of surface conduction (K_s). Additionally, at a given *n*, the normalized σ_{mix} increased with *S*, indicating the expansion of a diffuse double layer with *S* (Mojid and Cho 2006) and the consequent formation of a continuous electrical conduction path through the diffuse double layer.

Based on the difference between the measured σ_{mix} and estimated K_w from Eq. (16), K_s in unsaturated soils can be expressed by rearranging Eq. (11):

$$K_s = \sigma_{mix} - K_w = \sigma_{mix} - \sigma_w n^m S^{t_1} = \lambda(1 - n^m)S^{t_2} \quad (17)$$

To examine the impact of *S* on K_s, Eq. (17) was rearranged to define the unsat-sat K_s ratio:

$$\frac{\sigma_{mix} - \sigma_w n^m S^{t_1}}{\lambda(1 - n^m)} = S^{t_2} \quad (18)$$

Fig. 11(b) shows the variation of unsat-sat K_s ratio according to *S*. Based on the fitting between test results shown in Fig. 7 (i.e., results of saturated clays) and Eq. (10), the λ in Eq. (17) or (18) was determined to be 0.03 S/m for kaolin clay and 0.055 S/m for bentonite clays. In Fig. 11(b), the unsat-sat K_s ratio can be represented as a power function of *S*, with exponents of approximately 1.33 (for kaolin clay) and 1.56 (for bentonite clay), confirming the ability of Eq. (17) to capture the K_s of tested clays in unsaturated conditions. This reinforces the ability of Eq. (11) to capture the electrical conductivity of soils in unsaturated conditions.

The exponent for *S* in pore water conduction (K_w) (i.e., t_1 exponent in Eq. (11)) was comparable with that of previous studies (Hamada 2010; Mojid and Cho 2006; Pirson 1963). However, the *S* exponent in K_s (i.e., t_2 exponent in Eq. (11)) of tested clays was much smaller than that of previous studies, reinforcing that the *S* dependency of K_s of clayey soils differs from that of K_w (Fig. 11). In addition, it is notable that the t_2 exponent of the tested bentonite clay was greater than that of the tested kaolin clay, resulting in kaolin clay showing a greater unsat-sat K_s ratio at a given *S* (Fig. 11(b)). Because bentonite clay has a much larger specific surface than kaolin clay (Table 1), it can adsorb more water. Thus, to form the surface conduction network, bentonite clay requires more water, leading to a delayed increase in the unsat-sat K_s ratio with increasing *S* and the consequent greater t_2 exponent.

4.4. *Model verification*

This study extended the electrical conductivity model for saturated soils proposed by Glover et al. (2000) using a theoretical framework. The extended model, developed and expressed in this study as Eq. (11), can capture the electrical conductivity of unsaturated soils, and the validity of the extended model was assessed through experimental results performed at a very high pore water conductivity of approximately 4.2 S/m and a very low σ_w of approximately 0.012 S/m. Because the input parameters for Eq. (11) tabulated in Table 4 were determined based on these two conductivities, the experimental results performed at σ_w = 0.056, 0.51, 1.79, and 3.05 S/m (experimental data not used for model development) were used to verify the developed model and to confirm the findings.

Fig. 12 compares the measured and estimated values for σ_{mix}. The close agreement between those two, shown in Fig. 12, confirms the validity of Eq. (11). For quantitative evaluations, the mean absolute percentage error of 7.18 % (< 10 %) indicated a high degree of forecasting accuracy. In addition, Lin's Concordance Correlation Coefficient (CCC) was calculated for two soils to evaluate both the precision and accuracy of the estimated σ_{mix}. The determined CCC values for kaolin and bentonite clays were 0.996 and 0.973, respectively, indicating that the estimated σ_{mix} values for the two tested clays are strongly concordant with the measured values. As shown in Fig. 9, where the measured σ_{mix} was captured by the original Archie's equation, the exponent for *S* varied with σ_w. The good predictability of the developed model (Eq. (11)) with constant t_1 and t_2 exponents regardless of σ_w confirms that the paths for pore water conduction and surface conduction are not the same. Fig. 14 also confirms that the *m* exponent in Eq. (11) is not affected by *S*.

Additional model verification was performed using AMK clay, which was introduced in the Materials and Methodology section. The surface properties (i.e., specific surface) of AMK clay show an intermediate

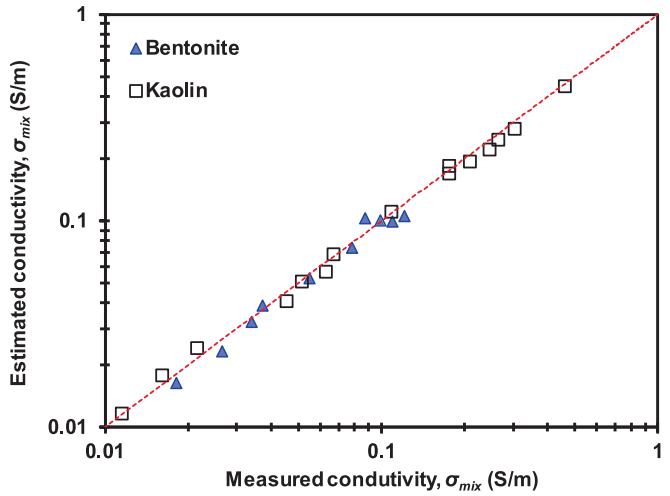

Fig. 12. Comparison between the measured and estimated electrical conductivities. The dashed line indicates the 1:1 line of agreement (estimated = measured).

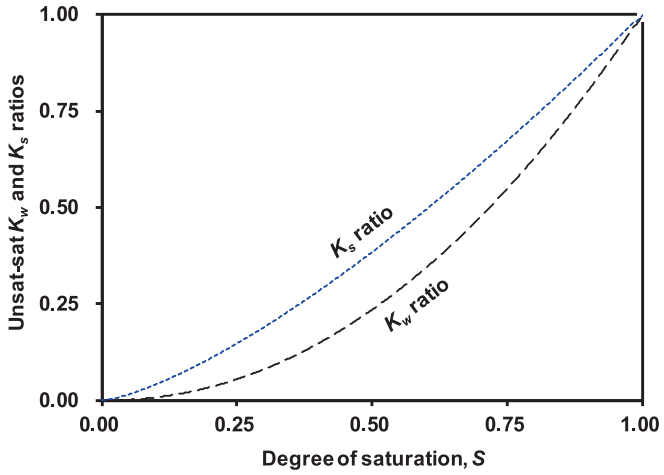

Fig. 13. Comparison between the unsaturated–saturated surface conduction (K_s) ratio (Equation (18)) and unsaturated–saturated pore water conduction (K_w) ratio (Equation (15)) of tested kaolin clay according to degree of saturation. Note, unsaturated–saturated K_s ratio = $S^{1.33}$ (Fig. 11(b)) and unsaturated–saturated K_w ratio = $S^{2.09}$ (Fig. 11(a)).

value between the kaolin and bentonite clays tested in this study (Table 1). Therefore, the dependencies of K_s and K_w on S for AMK clay are expected to lie between those of the kaolin and bentonite clays tested in this study. Fig. 10(e) and 10(f) show the normalized σ_{mix} (Eq. (12)) of the AMK clay with $S \sim 60$ % and 100 % as a function of n at high σ_w ($\sigma_w \sim 4.2$ S/m) and low σ_w ($\sigma_w \sim 0.012$ S/m), respectively. As previously explained, the normalized conductivity increased with increasing n in AMK clay under high-salinity pore water conditions, while it decreased with increasing n under low-salinity pore water conditions. However, the normalized conductivity increased with increasing S at a given n, regardless of the pore water conductivities.

By fitting the data from Fig. 10(e) with Eq. (15), the unsat-sat conductivity ratios were determined and plotted as a function of S in Fig. 11(a). The data points for AMK clay closely followed the trendline of kaolin clay. Additionally, by fitting the data from Fig. 10(f) with Eq. (18), using an input of $\lambda = 0.049$ S/m (Choo et al. 2022), the unsat-sat K_s ratios were determined and plotted as a function of S in Fig. 11(b). The data points for AMK clay fell between the trendlines of kaolin and bentonite clays, reinforcing the conclusion that K_s and K_w have different dependencies on S. The developed model, which incorporates separate S-exponents for K_w and K_s, provided accurate predictions of σ_{mix} across the test conditions, confirming the soundness of central hypothesis of this study.

5. Discussion

The experimental data in Fig. 11 demonstrates a fundamental difference in how electrical conduction evolves with increasing water saturation (S) for the two primary pathways in soil: pore water conduction (K_w) and surface conduction (K_s). Thus, for the thorough investigation of the different dependency of K_w and K_s on S, the unsat-sat K_w ratio for kaolin clay, which is $S^{2.09}$ (Fig. 11(a)), and the unsat-sat K_s ratio for kaolin clay, which is $S^{1.33}$ (Fig. 11(b)), were plotted as a function of S in Fig. 13. Fig. 13 clearly shows that the unsat-sat K_s ratio begins to increase at a much lower S compared to the unsat-sat K_w ratio. This is a critical finding, indicating that the conductive network for surface conduction forms and becomes continuous at lower moisture levels than the network for bulk pore water conduction.

This observation is rooted in the physical and chemical interactions between water and clay particles. As depicted in Fig. 14, the process of soil hydration occurs in a sequence of stages that provides a plausible explanation for our findings. Initially, water molecules are strongly adsorbed to the mineral surfaces, forming a tightly bound electrical double layer (Rashid et al. 2018). This initial layer of water, enriched with mobile ions, creates a pathway for surface conduction. As water content increases, this double layer expands, and the films of adsorbed water on adjacent particles eventually connect, forming a continuous electrical network for K_s. Only after this network is well-established and the moisture content of soil increases further does free water begin to fill the larger pore spaces between particles, forming capillary water and a continuous pathway for K_w. Therefore, as shown by experimental data in Fig. 13, the electrical conduction pathway for K_s becomes continuous and conductive at lower degrees of saturation than the pathway for K_w. This physical process explains why K_s has a smaller exponent for S than does K_w.

While our experiments, and the theoretical model, explore conditions down to very low saturations, it is important to note that under natural field conditions, the S of soils will rarely, if ever, reach zero. In reality, soils typically exist in a partially saturated state where both surface and pore water conduction are simultaneously active. Therefore, the total measured conductivity is a composite of these two parallel pathways, and the relative proportion of each is what dictates the overall electrical behavior. This proportion can be quantified directly using our proposed model (Eq. (11)) by calculating the contribution of each term to the total conductivity.

6. Conclusion and recommendations

A theoretical and experimental study was undertaken to develop a model of electrical conductivity (σ_{mix}) for unsaturated soils with varying magnitudes of pore water conduction (K_w) and surface conduction (K_s). A newly proposed σ_{mix} estimation formula, which incorporated separate saturation exponents for K_w and K_s, was verified using experimental results for sand and three types of clays. Thus, the distinct roles of K_w and K_s on σ_{mix} of unsaturated soils were explained, and an enhanced understanding of the electrical conductivity behavior of these soils was provided. This improved understanding can be used to inform more accurate modeling and prediction of soil behavior in various applications, such as soil characterization, soil hydrology, and environmental monitoring. Because the developed model can be used to describe the complex interplay between the measured electrical conductivity and soil/environmental properties such as matrix conductivity, porosity, degree of saturation, and pore water conductivity, the efficiency and reliability of site characterization and monitoring efforts can be enhanced, leading to more informed decision-making.

Further research is warranted to refine and validate the developed

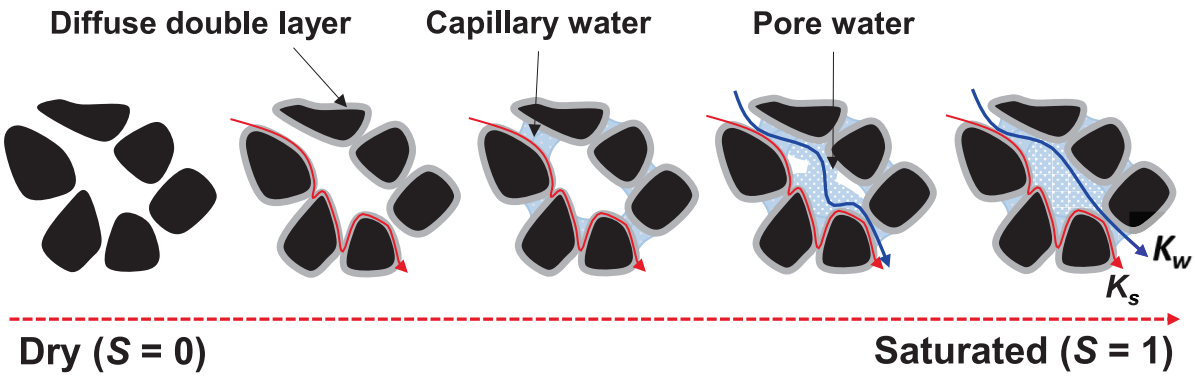

Fig. 14. Formation of electrical conduction network in soils with increasing degree of saturation.

model across a wider range of soil types, environmental conditions, and scenarios. Investigations of the influence of additional factors, such as soil structure, mineralogy, and temperature, on the electrical conductivity of unsaturated soils would contribute to a thorough understanding of soil behavior. Additionally, because this study only measured electrical conductivity in the horizontal direction, the effect of electrical anisotropy on the electrical conductivity of unsaturated soils could be another potential area for research. Finally, field-scale studies and long-term monitoring are needed to assess the applicability and robustness of the proposed model.

CRediT authorship contribution statement

Hyojung Ko: Writing – original draft, Methodology, Investigation. **Heerym Han:** Methodology, Investigation. **Hyunwook Choo:** Writing – review & editing, Supervision, Funding acquisition, Conceptualization.

Declaration of competing interest

The authors declare that they have no known competing financial interests or personal relationships that could have appeared to influence the work reported in this paper.

Acknowledgment

This work was supported by the National Research Foundation of Korea (NRF) grant funded by the Korean government (MSIT). RS-2023-00221719 and RS-2023-00208844

Data availability

Data will be made available on request.

References

Abu-Hassanein, Z.S., Benson, C.H., Blotz, L.R., 1996. Electrical resistivity of compacted clays. J. Geotech. Eng. 122 (5), 397–406. https://doi.org/10.1061/(ASCE)0733-9410(1996)122:5(397).

Archie, G.E., 1942. The electrical resistivity log as an aid in determining some reservoir characteristics. Transactions of the AIME 146 (01), 54–62. https://doi.org/10.2118/942054-G.

Atkins Jr, E., Smith, G.H., 1961. The significance of particle shape in formation resistivity factor-porosity relationships. J. Petrol. Tech. 13 (03), 285–291. https://doi.org/10.2118/1560-G-PA.

Bai, W., Kong, L., Guo, A., 2013. Effects of physical properties on electrical conductivity of compacted lateritic soil. J. Rock Mech. Geotech. Eng. 5 (5), 406–411. https://doi.org/10.1016/j.jrmge.2013.07.003.

Brovelli, A., et al., 2005. Electrical properties of partially saturated sandstones: novel computational approach with hydrogeophysical applications. Water Resour. Res. 41 (8). https://doi.org/10.1029/2004WR003628.

Chen, X., Kuang, L., Sun, Z., 2002. Archie parameter determination by analysis of saturation data. Petrophysics-the SPWLA Journal of Formation Evaluation and Reservoir Description 43 (02). https://doi.org/10.30632/PJV61N4-2020a2.

Choi, B., Kim, J., Choo, H., Won, J., 2025. Quantitative relation between particle shape and archie's cementation exponent for coarse grains: a statistical analysis. Results Eng. 27. https://doi.org/10.1016/j.rineng.2025.105794.

Choo, H., Burns, S.E., 2014. Review of Archie's equation through theoretical derivation and experimental study on uncoated and hematite coated soils. J. Appl. Geophys. 105, 225–234. https://doi.org/10.1016/j.jappgeo.2014.03.024.

Choo, H., et al., 2022. Estimating the electrical conductivity of clayey soils with varying mineralogy using the index properties of soils. Appl. Clay Sci. 217. https://doi.org/10.1016/j.clay.2021.106388.

Choo, H., et al., 2016a. Effects of clay fraction and pore water conductivity on electrical conductivity of sand-kaolinite mixed soils. J. Petrol. Sci. Eng. 147, 735–745. https://doi.org/10.1016/j.petrol.2016.10.009.

Choo, H., et al., 2016b. Impact of pore water conductivity and porosity on the electrical conductivity of kaolinite. Acta Geotech. 11 (6), 1419–1429. https://doi.org/10.1007/s11440-016-0490-4.

Chou, H., et al., 2012. Evaluation of solute diffusion tortuosity factor models for variously saturated soils. Water Resour. Res. 48 (10). https://doi.org/10.1029/2011WR011653.

Falleiros, M., et al., 1993. Neutron probe measurement of soil water content close to soil surface. Sci. Agric. 50, 333–337. https://doi.org/10.1590/S0103-90161993000300002.

Franco-Luján, V.A., et al., 2023. Reliability of electrical resistivity on the long-term monitoring of concrete. Results Eng. 18, 101154. https://doi.org/10.1016/j.rineng.2023.101154.

Fredlund, D.G., 2014. The emergence of unsaturated soil mechanics. Can. Geotech. J. 51 (12), ix–x. https://doi.org/10.1139/cgj-2014-0095.

Gens, A., 2010. Soil–environment interactions in geotechnical engineering. Géotechnique 60 (1), 3–74. https://doi.org/10.1680/geot.9.P.109.

Glover, P.W., Hole, M.J., Pous, J., 2000. A modified Archie's law for two conducting phases. Earth Planet. Sci. Lett. 180 (3–4), 369–383. https://doi.org/10.1016/S0012-821X(00)00168-0.

Hamada, G., 2010. Analysis of Archie's parameters determination techniques. Pet. Sci. Technol. 28 (1), 79–92. https://doi.org/10.1080/10916460802706463.

Hasan, M.F., Abuel-Naga, H., Leong, E.-C., 2021. A modified series-parallel electrical resistivity model of saturated sand/clay mixture. Eng. Geol. 290, 106193. https://doi.org/10.1016/j.enggeo.2021.106193.

Keller, G.V. and F.C. Frischknecht, *Electrical methods in geophysical prospecting.* 1966.

Klein, K.A., Santamarina, J.C., 2003. Electrical conductivity in soils: underlying phenomena. Journal of Environmental & Engineering Geophysics 8 (4), 263–273. https://doi.org/10.4133/JEEG8.4.263.

Ko, H., Choo, H., Ji, K., 2023. Effect of temperature on electrical conductivity of soils–Role of surface conduction. Eng. Geol. 321, 107147. https://doi.org/10.1016/j.enggeo.2023.107147.

Kohgo, Y., Nakano, M., Miyazaki, T., 1993. Theoretical aspects of constitutive modelling for unsaturated soils. Soils Found. 33 (4), 49–63. https://doi.org/10.3208/sandf1972.33.4_49.

Kułynycz, V., 2017. The influence of wettability on the petrophysical parameters of reservoir rocks. AGH Drilling. Oil, Gas 34 (3). https://doi.org/10.7494/drill.2017.34.3.775.

Kuranchie, F.A., Shukla, S.K., Habibi, D., 2014. Electrical resistivity of iron ore mine tailings produced in Western Australia. Int. J. Min. Reclam. Environ. 29 (3), 191–200. https://doi.org/10.1080/17480930.2014.941551.

Lee, H., Lee, J.-W., Oh, T.-M., 2021. Permeability evaluation for artificial single rock fracture according to geometric aperture variation using electrical resistivity. J. Rock Mech. Geotech. Eng. 13 (4), 787–797. https://doi.org/10.1016/j.jrmge.2021.04.003.

Liu, L., Li, W.L., Lu, Y.L., Ren, T.S., Horton, R., 2023. Relationship between thermal and electrical conductivity curves of soils with a unimodal pore size distribution: Part 1. a unified series-parallel resistor model. Geoderma 432. https://doi.org/10.1016/j.geoderma.2023.116420.

Liu, L., Lu, Y.L., Fu, Y.W., Horton, R., Ren, T.S., 2022. Estimating soil water suction from texture, bulk density and electrical resistivity. Geoderma 409. https://doi.org/10.1016/j.geoderma.2021.115630.

McCarter, C.P.R., Rezanezhad, F., Quinton, W.L., Gharedaghloo, B., Lennartz, B., Price, J., Connon, R., Van Cappellen, P., 2020. Pore-scale controls on hydrological

and geochemical processes in peat: Implications on interacting processes. Earth Sci. Rev. 207. https://doi.org/10.1016/j.earscirev.2020.103227.
Millington, R., Quirk, J., 1961. Permeability of porous solids. Trans. Faraday Soc. 57, 1200–1207. https://doi.org/10.1039/TF9615701200.
Mojid, M., Cho, H., 2006. Estimating the fully developed diffuse double layer thickness from the bulk electrical conductivity in clay. Appl. Clay Sci. 33 (3–4), 278–286. https://doi.org/10.1016/j.clay.2006.06.002.
Mualem, Y., Friedman, S., 1991. Theoretical prediction of electrical conductivity in saturated and unsaturated soil. Water Resour. Res. 27 (10), 2771–2777. https://doi.org/10.1029/91WR01095.
Mufti, S., Das, A., 2023. Modeling unsaturated hydraulic conductivity of granular soils using a combined discrete element and pore-network approach. Acta Geotech. 18 (2), 651–672. https://doi.org/10.1007/s11440-022-01597-3.
Nocco, M.A., Ruark, M.D., Kucharik, C.J., 2019. Apparent electrical conductivity predicts physical properties of coarse soils. Geoderma 335, 1–11. https://doi.org/10.1016/j.geoderma.2018.07.047.
Ozgur, M., 2023. Development and validation of a degree of saturation prediction model using time domain reflectometry for compaction control. Transp. Geotech. 42, 101062. https://doi.org/10.1016/j.trgeo.2023.101062.
Pfannkuch, H.O., 1972. On the correlation of electrical conductivity properties of porous systems with viscous flow transport coefficients. Dev. Soil Sci. 2, 42–54. https://doi.org/10.1016/S0166-2481(08)70527-0.
Pirson, S.J., *Handbook of well log analysis for oil and gas formation evaluation.* 1963.
Rashid, Q.A., et al., 2018. Experimental-artificial intelligence approach for characterizing electrical resistivity of partially saturated clay liners. Appl. Clay Sci. 156, 1–10. https://doi.org/10.1016/j.clay.2018.01.023.
Salem, H.S., Chilingarian, G.V., 1999. The cementation factor of Archie's equation for shaly sandstone reservoirs. J. Petrol. Sci. Eng. 23 (2), 83–93. https://doi.org/10.1016/S0920-4105(99)00009-1.
Samouëlian, A., Cousin, I., Tabbagh, A., Bruand, A., Richard, G., 2005. Electrical resistivity survey in soil science: a review. Soil till Res 83 (2), 173–193. https://doi.org/10.1016/j.still.2004.10.004.
Sangprasat, K., Puttiwongrak, A., Inazumi, S., 2024. Comprehensive analysis of correlations between soil electrical resistivity and index geotechnical properties. Results Eng. 23, 102696. https://doi.org/10.1016/j.rineng.2024.102696.
Santamarina, J., Klein, K., Wang, Y.-H., Prencke, E., 2002. Specific surface: determination and relevance. Can. Geotech. J. 39 (1), 233–241. https://doi.org/10.1139/t01-077.
Scarfone, R., Wheeler, S.J., Lloret-Cabot, M., 2020. Conceptual hydraulic conductivity model for unsaturated soils at low degree of saturation and its application to the study of capillary barrier systems. J. Geotech. Geoenviron. Eng. 146 (10), 04020106. https://doi.org/10.1061/(ASCE)GT.1943-5606.0002357.
Schön, J.H., *Physical properties of rocks: Fundamentals and principles of petrophysics*. 2015: Elsevier.
Sharma, A., Singh, B., Sandhu, B., 2017. A gamma-ray scattering technique for estimation of density and moisture content of wood. Radiat Eff. Defects Solids 172 (3–4), 286–295. https://doi.org/10.1080/10420150.2017.1307193.
Sheng, D., 2011. Review of fundamental principles in modelling unsaturated soil behaviour. Comput. Geotech. 38 (6), 757–776. https://doi.org/10.1016/j.compgeo.2011.05.002.
Talabani, S., et al., *Validity of Archie equation in carbonate rocks.* Abu Dhabi International Petroleum Exhibition and Conference, 2000: p. SPE-87302-MS. https://doi.org/10.2118/87302-MS.
Wahba, M., et al., 2024. Experimental characterization of contact resistance of desert soil with waste-enhancement materials in grounding systems. Results Eng. 23, 102707. https://doi.org/10.1016/j.rineng.2024.102707.
Yang, Y.-S., et al., 2024. Assessing shallow slope stability using electrical conductivity data and soil hydraulic characteristics. Eng. Geol. 331, 107447. https://doi.org/10.1016/j.enggeo.2024.107447.
Zhang, X., et al., 2024. Machine learning prediction model for clay electrical conductivity and its application in electroosmosis consolidation. Acta Geotech. 19 (10), 6553–6568. https://doi.org/10.1007/s11440-024-02411-y.
Zhong, Z., et al., 2022. The salinity dependence of electrical conductivity and Archie's cementation exponent in shale formations. J. Petrol. Sci. Eng. 208, 109324. https://doi.org/10.1016/j.petrol.2021.109324.
Zhou, M., et al., 2015. Laboratory investigations on factors affecting soil electrical resistivity and the measurement. IEEE Trans. Ind. Appl. 51 (6), 5358–5365. https://doi.org/10.1109/TIA.2015.2465931.